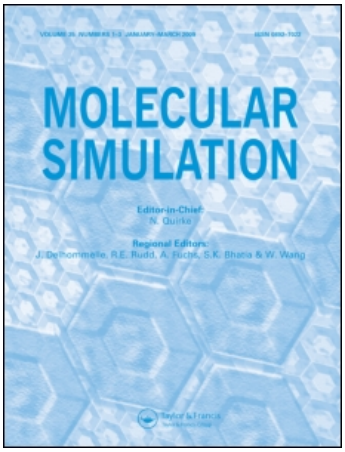

Molecular Simulation
Publication details, including instructions for authors and subscription information:
http://www.informaworld.com/smpp/title~content=t713644482

Molecular Dynamics Simulations of Langmuir-Blodgett Monolayers with Explicit Head-group Interactions

K. S. Kim[a]; M. A. Moller[a]; D. J. Tildesley[a]; N. Quirke[ab]
[a] Department of Chemistry, The University, Southampton, U.K. [b] European Centre for Computational Science and Technology, Biosym Technologies, Parc Club Orsay Université, Orsay, Cedex, France

To cite this Article Kim, K. S. , Moller, M. A. , Tildesley, D. J. and Quirke, N.(1994) 'Molecular Dynamics Simulations of Langmuir-Blodgett Monolayers with Explicit Head-group Interactions', Molecular Simulation, 13: 2, 77 — 99
To link to this Article: DOI: 10.1080/08927029408021976
URL: http://dx.doi.org/10.1080/08927029408021976

Molecular Simulation, 1994, Vol. 13, pp. 77-99
Reprints available directly from the publisher
Photocopying permitted by license only

MOLECULAR DYNAMICS SIMULATIONS OF LANGMUIR-BLODGETT MONOLAYERS WITH EXPLICIT HEAD-GROUP INTERACTIONS

K.S. KIM, M.A. MOLLER, D.J. TILDESLEY and N. QUIRKE†

Department of Chemistry, The University, Southampton S09 5NH, U.K.

(Received June 1993, accepted September 1993)

Energy minimisation and molecular dynamics calculations have been performed for models of Langmuir-Blodgett films containing stearic acid molecules. The model includes a specific representation of the atoms and dipole moment of the carboxylic acid head-group. Simulations have been performed at head-group areas per molecule of 20.6 $Å^2$ and 21.2 $Å^2$ at room temperature. This all-atom model predicts significant conformational disorder at the torsional angle connecting the head-group to the hydrocarbon chain. The strong charge/image-charge interaction doubles the tilt of the layer over that found for the united-atom Lennard-Jones head-group. The dipoles of the head-group are aligned parallel to the surface forming a two sub-lattice structure in the plane of the surface.

KEY WORDS: Langmuir-Blodgett films, stearic acid, tilting transition

1 INTRODUCTION

A recent review of Langmuir-Blodgett films [1] demonstrates the wide range of experimental techniques which have now been used to study the structure and dynamics of amphiphilic molecules physically and chemically adsorbed on surfaces. Molecular simulation has a key rôle to play in these experiments since the molecular interpretation of the raw data in experiments such as fluorescence depolarisation, NEXAFS and atomic force microscopy is often highly model dependent. The simulation can test the assumptions which are at the root of these experimental "models". In addition the simulation offers a unique opportunity to perform hamilitonian surgery: the technique of deliberately removing or adding parts of a realistic model of the intermolecular forces to understand the effect that these forces have on the overall property of the film. For example, it is interesting to change the dihedral potential governing the conformational behaviour of the hydrocarbon chain so that amphiphiles can only exist in the *all-trans* configuration. The comparison of this simulation with that of the full potential model adds to our understanding of the part played by molecular flexibility in determining the overall tilt of the layer [2]. An understanding of the importance of each part of the hamiltonian in determining the properties of the film is the first step to designing materials with particular structural and electronic properties and to realising the significant number of potential applications discussed by Roberts [1].

† Address for correspondence: European Centre for Computational Science and Technology, Biosym Technologies Sarl, Parc Club Orsay Université, 20, rue Jean Rostand, 91893 Orsay Cedex, France.

Some progress has already been made in this direction. The earliest simulations of monolayers and bilayers used a "united-atom" representation of the methylene groups in the hydrocarbon chain [3, 4]. The ϵ and σ parameters used to characterise the dispersion-repulsion interaction between methylene groups were taken from earlier studies of liquid butane and liquid decane [5]. Early simulations of amphiphiles on solids (Langmuir-Blodgett films) [6, 7] and amphiphiles on water (Langmuir films) [8] used these parameters. There is now a growing body of evidence from energy minimisation studies [9, 2] and from molecular dynamics simulations that the explicit interactions between the hydrogen atoms in the chain determine the range of head-group areas per molecule over which the collective tilt changes from $\approx 30°$ to upright and may also determine the relative stabilities of a collective tilt towards nearest-neighbour or next-nearest-neighbour molecules in the same layer. The commonly used σ parameter for the diameter of the "united atoms" methylene group [5] certainly underestimates the effective diameter of the longer chains in the Langmuir-Blodgett monolayer.

Although the importance of including a realistic representation of the hydrocarbon chain is established, the models used to represent the hydrophilic portion of the amphiphile have, in most cases, been quite unrealistic. A number of workers [6, 7, 10] have simply ignored the head-group to concentrate on the structure induced by the packing of the hydrocarbon chains. Others, including ourselves, [2, 3, 4, 8] have represented the repulsion-dispersion interaction between head-groups as a united-atom Lennard-Jones potential. In these studies the electrostatic interaction between head-groups and between the head-group and the surface has been ignored. A number of studies of the adsorbed alkanethiols ($C_nH_{2n+1}SH$) on the Au(111) surface [9, 11] have recognised that the sulphur head-groups are chemically adsorbed at fixed sites on the surface. Again the sulphur-sulphur lateral interaction is represented by a Lennard-Jones interaction with the σ parameter chosen to be sufficiently large to lock the molecules into the triangular commensurate lattice. There have been two studies which have explicitly attempted to handle the dipolar interactions between the molecules. Fois and Madden [12] have studied patches of stearic acid molecules using Monte Carlo techniques. The chains and head-groups in these amphiphiles are rigid and fixed rigidly with respect to one another. Hautman *et al.* [13] have studied adsorbed alkanethiols with polar tail-groups (i.e. $HS(CH)_nX$ with $X = -OH$ or $-C\equiv N$).

This paper attempts to model completed monolayers of stearic acid molecules on a structureless surface. It is a systematic extension of the work presented in reference [2] and we have developed the explicit-hydrogen representation of the chain to include a more realistic representation of the head-group. The all-atom representation of the carboxylic acid head-group includes a dipole-dipole interaction modelled using partial charges. Torsional potentials are used to control the relative orientation of the plane of the backbone and the plane of the head-group. The hydrophilic interaction between the head-group and the surface is represented using an attractive dispersion interaction and an image charge interaction between the dipole and the underlying dielectric medium. The aim of the work is to understand the effect of the head-group on the structure of the film by a careful comparison with the results of the simpler model reported in [2].

Section 2 describes the potential model used to represent the adsorbed stearic acid. Section 3 is an energy minimisation study of this model which excludes conformational changes. These studies are an essential prerequisite to the more expensive

molecular dynamics simulations reported in section 4. Two molecular dynamics simulations are performed at room temperature and head-group areas per molecule close to the experimentally observed deposition densities. The translational, orientational and conformational structure of the film are discussed in detail. Section 6 contains our conclusions.

2 THE POTENTIAL MODEL

2.1 *The Intramolecular and Intermolecular potentials*

The stearic acid molecule is composed of a methyl tail-group, 16 methylene groups ($-CH_2-$) and a carboxylic acid head-group ($-COOH$). In our potential model the bond-lengths are rigidly constrained to their equilibrium values. The bond-angles are controlled by harmonic potentials of the form

$$V_\theta(\theta) = \frac{1}{2}k_\theta(\theta - \theta_0)^2. \tag{1}$$

The equilibrium bond-lengths, bond-angles and constants k_θ are contained in Table 1. The methylene groups in the hydrocarbon chains are rigidly constrained so that the plane containing the hydrogen atoms H1 and H2 and the carbon atom C2 is perpendicular to the plane containing the atoms C1, C2 and C3 (see Figure 1). The atoms around the sp2 carbon C1 are constrained to be co-planar using the method of vector constraints [14]. The conformation of the hydrocarbon chain is controlled by the dihedral potential of Ryckaert and Bellemans [15] which has the functional form

$$V_{RB}(\phi) = \sum_{n=1}^{n_{max}} c_i \cos^i\phi. \tag{2}$$

There are eight dihedral potentials controlling the conformation of the head-group with respect to the chain. These eight potential can be reduced since the relative orientations of the methylene hydrogens and the carbon backbone are fixed. Thus the dihedral potentials which controls the conformation of the four atoms O1, C1, C2 and C3 and O2, C1, C2 and C3 are V_I and V_{II} respectively.

Table 1 The bond-length and bond-angle parameters used to define the equilibrium geometry of the stearic acid molecule. The parameters for the hydrocarbon chain are from reference [2] where the HCH bond-angle is rigidly constrained. The parameters for the head-group are taken from the AMBER force field [14]. The atom definitions are shown in Figure 1.

Bond-length		*Bond-angle: θ_0*		*K_θ/kJ mol^{-1}*
r_{C-C}/Å	1.53	⟨C−C−C/°	109.5	520
r_{C-H}/Å	1.04	⟨H−C−H/°	106	*rigid*
r_{C1-O1}/Å	1.364	⟨O1−C1−C/°	109	335
r_{C1-O2}/Å	1.25	⟨O2−C1−C/°	125	335
r_{O1-H}/Å	0.96	⟨O1−C1−O2/°	124	335
		⟨HD−O1−C1/°	113	146

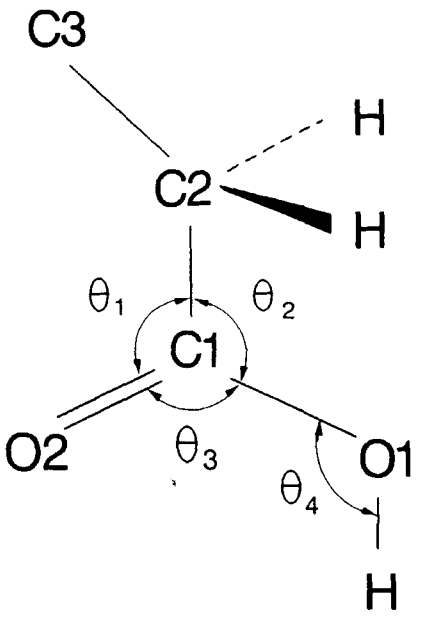

Figure 1 The atom types used in defining the intermolecular and intramolecular potentials. The dihedral potentials $V_{RB}(\phi)$ and $V_I(\phi) + V_{II}(\phi)$ control the conformational behaviour around the bonds marked ϕ_{RB} and ϕ_{I+II} respectively.

$$\begin{aligned} V_I(\phi) &= V_{O1C1C2C3}(\phi) + V_{O1C1C2H1}(\phi - 120) + V_{O1C1C2H2}(\phi + 120) \\ V_{II}(\phi) &= V_{O2C1C2C3}(\phi) + V_{O2C1C2H1}(\phi - 120) + V_{O2C1C2H2}(\phi + 120) \end{aligned} \tag{3}$$

where the atom types are shown in Figure 1. The two dihedral potentials V_I and V_{II} control the relative orientation of the plane containing the first three carbon atoms of the hydrocarbon chain and the plane of the head-group. Two other dihedral potentials $V_{HO1C1C2}(\phi)$ and $V_{HO1C1O2}(\phi)$ are required to define the orientation of the hydroxyl hydrogen with respect to the head-group plane. The parameters for these four potentials are given in Table 2.

Repulsion-dispersion interactions between atoms within the same chain are modelled using the Lennard-Jones potential

$$V_{LJ}(r_{\alpha\beta}) = 4\epsilon_{\alpha\beta}\left[\left(\frac{\sigma_{\alpha\beta}}{r_{\alpha\beta}}\right)^{12} - \left(\frac{\sigma_{\alpha\beta}}{r_{\alpha\beta}}\right)^{6}\right] \tag{4}$$

In our previous paper [2] we developed an explicit hydrogen model where the individual atoms in two methylene groups separated by more than three carbon atoms interact through nine separate Lennard-Jones interactions. The terminal methyl group in the chain is treated as a united atom. The ϵ and σ parameters for this 1–5 interaction are given in Table 3. The parameters for the crossed interactions, such as that between a hydrogen and carbon atom, are obtained using the normal mixing rules.

Table 2 The torsional potential parameters in eqn (2). (a) [14], (b) [15].

Atom types	*torsional potential parameters*
C1−C2−C3−C4[(a)]	$c_0 =$ 9.2789
	$c_1 =$ 12.1557
	$c_2 =$ −13.1201
	$c_3 =$ −3.0579
	$c_4 =$ 26.2403
	$c_5 =$ −31.4950
O1−C1−C2−C3[(b)]	$c_0 =$ −0.151
V_I	$c_1 =$ −0.353
	$c_2 =$ 0.30
	$c_3 =$ 0.204
O2−C1−C2−C3[(b)]	$c_0 =$ 0.597
V_{II}	$c_1 =$ −0.2435
	$c_2 =$ −0.904
	$c_3 =$ 0.30
HD−O1−C1−C2	$c_0 =$ 0.50
	$c_1 =$ 0.0
	$c_2 =$ −0.5
	$c_3 =$ 0.0
HD−O1−C1−O2	$c_0 =$ 3.9575
	$c_1 =$ 1.6425
	$c_2 =$ −5.60
	$c_3 =$ 0.0.

Table 3 Potential parameters for atoms in the stearic acid molecule. a: carbon and hydrogen in methylene group. b: carbon atom in head-group. c: hydroxyl oxygen atom in head group. d: carbonyl oxygen atom in head-group. e: hydrogen atom in head group. $1|e| = 1.60218 \times 10^{-19}$ C.

Site	$\epsilon/kJ\,mol^{-1}$	$\sigma/\text{Å}$	*Mass/amu*	$q_\alpha/\|e\|$
CH_3	0.64230	3.740	15.035	–
C[a]	0.40561	2.908	12.011	–
H[a]	0.05683	2.908	1.008	–
C1[b]	0.50209	3.296	15.035	0.575
O1[c]	0.62760	2.940	15.995	−0.350
O2[d]	0.83683	2.850	15.995	−0.450
H(D)[e]	0.08368	1.782	2.016	0.225

$$\epsilon_{\alpha\beta} = (\epsilon_{\alpha\alpha}\epsilon_{\beta\beta})^{1/2}$$
$$\sigma_{\alpha\beta} = \frac{1}{2}(\sigma_{\alpha\alpha} + \sigma_{\beta\beta}) \qquad (5)$$

The repulsion-dispersion interactions for atoms in the head-group are taken from the MM2 force field [16] and are given in Table 3. The four atoms in the head-group interact with atoms in the chain belonging to the methylene group C4 and above (see Figure 1). There is a direct repulsion-dispersion interaction between the carboxyl oxygen O2 and the hydroxyl hydrogen (HD) of the head-group.

The values of the partial charges [17] on the four atoms of the head-group are given in Table 3. These charges give rise to an overall dipole moment of 1.79D[1]. There is a direct interaction

[1] $1D = 3.33564 \times 10^{-30}$ C m.

$$V_{cc}(r_{\alpha\beta}) = \frac{q_\alpha q_\beta}{4\pi\epsilon_0 r_{\alpha\beta}} \tag{6}$$

between the partial charges on O2 and HD. This unusual intramolecular charge-charge interaction keeps the O2 and HD groups of the carboxylic acid in the cis configuration for all of the molecules throughout the dynamics calculation.

Each atom in a molecule interacts with all atoms in other molecules through the Lennard-Jones dispersion-repulsion interaction. These short-range interactions are handled within the minimum image convention without the use of a potential cut-off. Partial charges within the head-group interact with partial charges in other head-groups. The use of the minimum image convention with the long-range dipolar interaction is avoided by the implementation of a cylindrical cut-off. The radius of the cut-off circle in the plane of the surface is half the length of the shortest side of the simulation box. The effect of this cut-off is discussed in section 3. Since the completion of this work Hautman and Klein have suggested a useful Ewald technique which can be used in the simulation of Langmuir Blodgett films [18].

2.2 *The molecule surface potential*

Each atom in the stearic acid molecule interacts with the structureless surface(s) through an integrated Lennard-Jones 9-3 potential.

$$V_{\alpha s}(z_\alpha) = \frac{2\pi\hat{n}}{3}\epsilon_{\alpha s}\left[\frac{2}{15}\left(\frac{\sigma_{\alpha s}}{z_\alpha}\right)^9 - \left(\frac{\sigma_{\alpha s}}{z_\alpha}\right)^3\right] \tag{7}$$

where $\hat{n} = 0.114\,\text{Å}^{-3}$ is the density of the solid, $\epsilon_{ss} = 28\,\text{K}$ and $\sigma_{ss} = 3.4\,\text{Å}$ [2]. These parameters are appropriate to a graphitic carbon surface. An image charge interaction is used to model the attraction between the head-group and the hydrophilic surface. The partial charges create image charges in an image plane. In a continuum model the image plane is located at the point where the relative permittivity changes discontinuously from ϵ' (in the surface) to ϵ (above the surface). The position of the image plane for an atomic surface is uncertain and we have followed the normal practice of locating the plane at $z_{ip} = \sigma_{ss}/2$ [19]. The interaction between a charge and its image is

$$V_{ic}(z) = \frac{1}{2}\frac{(\epsilon - \epsilon')}{(\epsilon + \epsilon')}\left[\frac{q_\alpha^2}{8\pi\epsilon_0(z - z_{ip})}\right] \tag{8}$$

The value of $\epsilon' = 4.0$ (which is appropriate for quartz glass [20]) produces an image charge which reduced with respect to the real charge by a factor of $(\epsilon - \epsilon')/(\epsilon + \epsilon') = -0.6$.) A charge interacts with its own image and with images of other charges. There is no interaction between image charges.

3 ENERGY MINIMISATION

Energy minimisation calculations have been performed on the model discussed in section 2 for a variety of head-group areas per molecules. The head groups of the stearic acid molecules were fixed in a triangular lattice on the surface and the hydrocarbon chains were fixed in the all-trans configuration.

Table 4 Effect of system size on the energy minimisation calculation. $\langle V_{cc} \rangle$ is the electrostatic energy per molecule and θ_{tilt} is the tilt angle of the layer at the particular head-group area.

System Size	$A_m = 20.6$ Å^2		$A_m = 21.2$ Å^2	
	$\langle V_{cc} \rangle$/kJ mol^{-1}	θ_{tilt}/°	$\langle V_{cc} \rangle$/kJ mol^{-1}	θ_{tilt}/°
6 × 6	−3.320	0.0	−3.001	30.61
8 × 8	−3.329	0.0	−3.092	30.43
10 × 10	−3.385	0.12	−3.174	30.38

The NAG library routine E04JBF was used to minimise the total energy, calculated using the minimum image convention, with respect to the orientation of the molecules. This routine is a quasi-Newton algorithm for finding an unconstrained minimum of a function of several variables. The details of the calculation are discussed in [2]. The minimisations were performed using both one and two molecules per unit cell. The minimum energy structures were calculated with and without the electrostatic interactions between the partial charges in head groups. The electrostatic interactions were calculated using a cylindrical cut-off. The radius of the cut-off circle in the plane of the surface was fixed at half the length of the shortest side of the periodic box. Molecules contribute to the electrostatic interaction if the carbon atom of the head-group is within the cut-off circle. We have not applied an Ewald sum in this geometry but the effect of the truncation can be judged by considering the results of the energy minimisation for a number of system sizes presented in table 4. As one might expect increasing the system size increases the magnitude of the electrostatic interaction; the total change in the electrostatic interaction in changing from a 6 × 6 to a 10 × 10 system is 0.5% of the total configurational energy. More importantly, the tilt angle of the molecules is not significantly changed by increasing the system size. The energy minimisation and molecular dynamics calculation were performed using the 8 × 8 system. Recent system size studies of similar systems by Bishop and Clarke [21] conclude that studies of 64 molecules per layer produce statistically significant results on molecular tilt.

Figures 2 and 3 show the minimum energy, E_{min}, and the molecular tilt with respect to the surface normal at the minimum energy, θ_{min}, as a function of the head-group area per molecule, A_m. Results are shown for the model with and without the electrostatic interactions.

The results of the energy minimisation are summarised in Tables 5 and 6. The angle ψ is the third Euler angle describing the twist of the molecule around its long-axis. The angle is defined in equation (11). Where there are two distinct values of ψ, this indicates a two sublattice struture in which half the molecules exhibit a different twist angle. The calculations for the models with and without electrostatic interactions are quite similar and the energy-minimised monolayer structures of the all-atom-head-group model developed in this paper are also similar to those found for the single-atom head-group model of reference [2]. (In this model the carboxylic acid head group was considered as a single Lennard-Jones interaction site). In the single-atom head-group model the tilt occurs at $A_m = 20.6$Å^2 in the all-atom-head-group model at $A_m = 20.8$Å^2. This difference reflects the larger effective cross-section of the all-atom-head-group compared with that of the single-atom-head-group. The minimum energy monolayer structures have one molecule

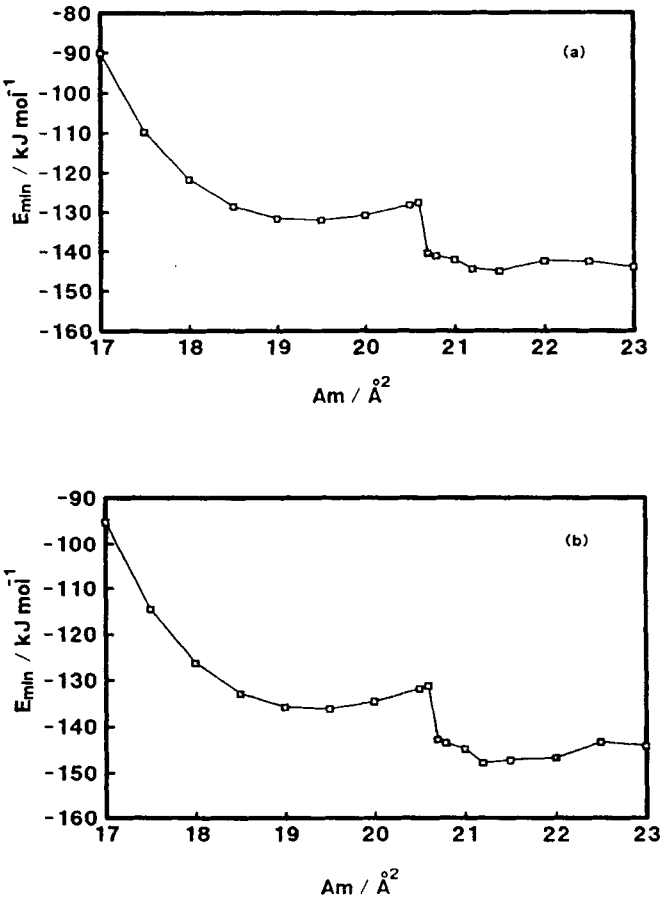

Figure 2 The minimum energy, E_{min}, as a function of the head-group area per molecule, A_m: (a) without electrostatic interactions; (b) with electrostatic interactions.

Table 5 Results of the energy minimisation without electrostatic interactions.

Head-group Area/ Å^2	ϕ_{min}/°	θ_{min}/°	$\psi_{min,1}$/°	$\psi_{min,1}$/°	U_{min}/kJ mol^{-1}
17	0	0	0	0	−95.207
18	0	0	0	0	−121.770
19	0	0	0	0	−131.597
20	0	0	0	0	−130.767
20.7	89.9	28.9	136.1	224.1	−140.487
22	90.8	33.1	135.7	222.3	−145.028
23	78.6	37.3	233.6	233.6	−142.602

per unit cell for $A_m < 20.6$ Å^2 and $A_m \geq 23$ Å^2, but two molecules per unit cell in the region 20.6 Å$^2 \leq A_m < 23$ Å^2. This result was also seen for the single-atom head-group model. In summary, within the approximations of this rigid model, the electrostatic interaction between head groups has a very small effect on the static

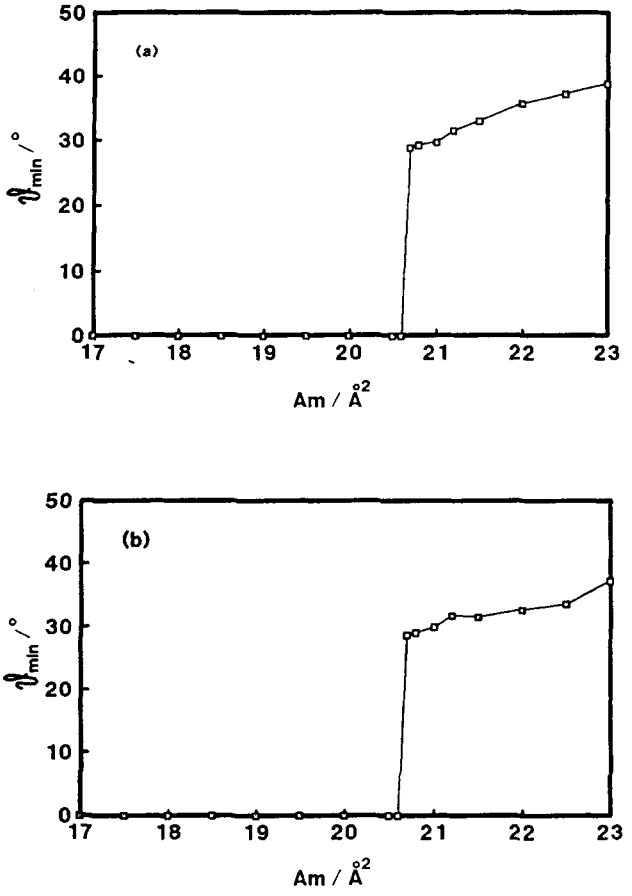

Figure 3 The molecular tilt with respect to the surface normal at the minimum energy, θ_{min}: (a) without electrostatic interactions; (b) with electrostatic interactions.

Table 6 Results of the energy minimisation without electrostatic interactions.

Head-group Area/ Å^2	ϕ_{min}/°	θ_{min}/°	$\psi_{min,1}$/°	$\psi_{min,1}$/°	U_{min}/kJ mol^{-1}
17	0	0	0	0	−95.207
18	0	0	0	0	−126.286
19	0	0	0	0	−132.899
20	0	0	0	0	−134.518
20.7	89.9	28.7	135.8	224.3	−142.670
22	90.1	32.8	136.7	223.1	−146.595
23	79.7	37.4	230.9	230.9	−143.996

minimum energy structure at 0 K. Although the electrostatic energy of the layer is less than 5% of the total energy of the layer (which is dominated by the dispersion interaction of the alkyl chains), it is the relative sizes of these two contributions as a function of tilt angle which will determine the overall tilt of the layer. Certainly

in the case where the conformation of the head-group is fixed relative to the chain, the results are almost unchanged from the results of the explicit hydrogen model. However, it is possible that the strong charge/image-charge interaction and the conformational freedom of the head-group will allow different structures to develop at room temperature. The constraint of keeping the molecules fixed in the all-trans configuration is most easily relaxed by moving to a full molecular dynamics calculation of the system.

4 MOLECULAR DYNAMICS

The molecular dynamics simulations of 64 molecules were carried out using the Verlet algorithm [22]. During the simulation the bond length of the molecules were constrained to their equilibrium value using SHAKE algorithm and the plane containing the 3 atoms of methylene ($-CH_2-$) group is constrained to be normal to the plane of the three nearest carbon atoms of alkyl chain. The vector bisecting the H—C—H bond-angle in each methylene group is constrained to be co-linear with the vector bisecting the corresponding C—C—C angle: further details of these constraints are given in [2]. The atoms O2, C1 and O1 of the head-group are constrained to be co-planar and the d_{CO1}, d_{CO2}, and d_{O1H}, bond-lengths are constrained to their experimental values. A monolayer of 64 stearic acid molecules in the all-trans configuration was placed on a hydrophilic surface with the head-groups in a triangular lattice. The orientation of the molecules was chosen to correspond to the minimum energy configuration at that head-group area per molecule. Two molecular dynamics simulations were performed at head-group areas $A_m = 20.6\text{Å}^2$ and $A_m = 21.2\text{Å}^2$. The these two densities are chosen to be on either side of the tilt transition observed in the energy minimisation calculations. We performed an equilibration run of 30,000 steps (60 ps) and a production run of 35,000 steps (70 ps) steps for the system at $A_m = 20.6\text{Å}^2$ and an equilibration of 39,000 steps (78 ps) followed by a production run of 49,000 steps (98 ps) for the system at $A_m = 21.2\text{Å}^2$. After equilibration, runs of 40 ps are required in this type of calculation to obtain statistically meaningful results [21]. Both of the simulations were started at a temperature of 298 K. Total energy is conserved to 1 part in 10^4 throughout the production phase of the calculation and there is no overall drift in the calculated averages.

Snapshots of the instantaneous structure of the stearic acid monolayer from three orthogonal directions are shown in Figure 4 for $A_m = 20.6\text{Å}^2$ and $A_m = 21.2\text{Å}^2$.

4.1 *The translational structure of the stearic acid monolayer*

The translational structure of the monolayers has been characterised by calculating the radial distribution function, g(r) of the centre of mass of the molecules. This is effectively a two dimensional distribution function and in normalised appropriately. Figure 5 shows g(r) at $A_m = 20.6\text{Å}^2$ and $A_m = 21.2\text{Å}^2$. Both distribution functions are characteristic of a solid structure with distinct first and second peaks and pronounced structures out to intermolecular separations of 20 Å. The hexagonal nature of the solid can be measured by calculating an hexagonal order parameter (OP_{hex}) as a function of time. OP_{hex} is defined as

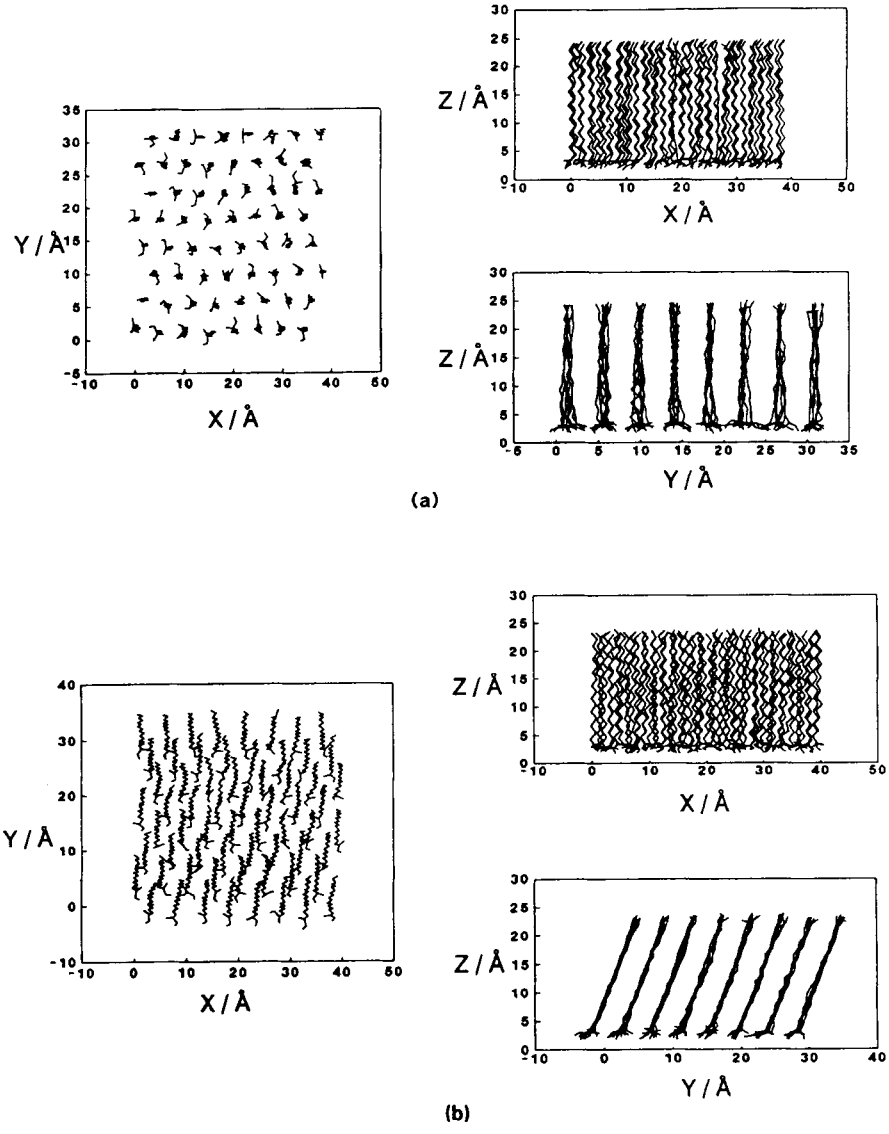

Figure 4 A snapshot of the instantaneous structure of the stearic acid monolayer from three orthogonal directions: (a) $A_m = 20.6$ Å^2; (b) $A_m = 21.2$ Å^2.

$$\mathrm{OP}_{hex} = \left\langle \tfrac{1}{6} \sum_{i=1}^{6} \exp(i6\theta_i) \right\rangle \tag{9}$$

where θ_i is the angle between vectors from the centre of mass of molecule to the centre of mass of two adjacent nearest neighbour molecules (see the sketch in Figure 6). The projection of the intermolecular vectors onto the surface is used in the

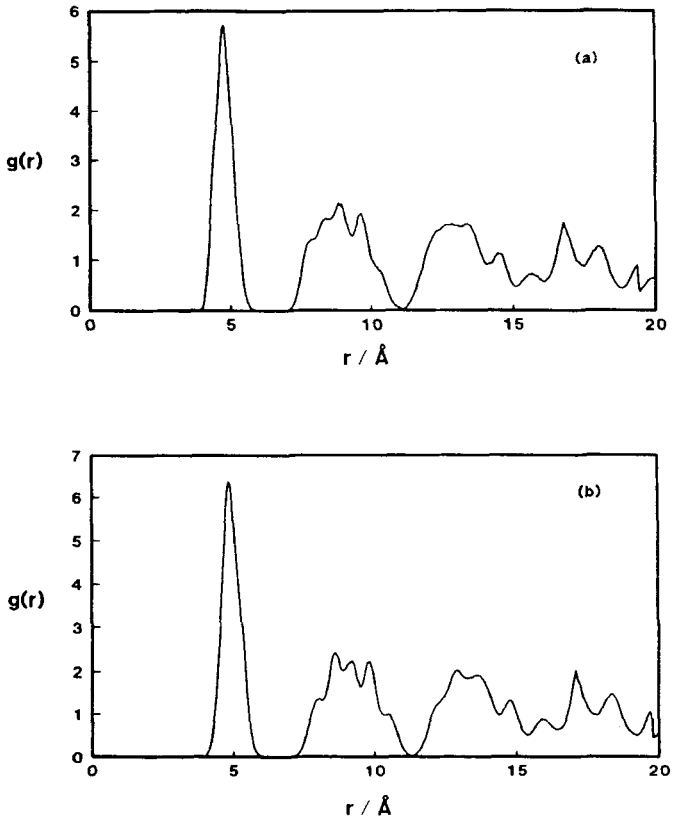

Figure 5 The radial distribution function of the centre-of-mass of the adsorbed stearic acid molecules: (a) A_m = 20.6 Å^2; (b) A_m = 21.2 Å^2.

calculation of the order parameter which is averaged over all the molecules. Figure 6 shows OP_{hex} as a function of time for both densities. Both systems exhibit relatively high values of $OP_{hex} = 0.8 \pm 0.02$ throughout the production phase of the simulation. A 5% rectangular distortion of the structure gives would produce a value of $OP_{hex} = 0.77$. Both monolayers exhibit a well-ordered hexagonal structure which is more strongly developed than that found with the single-atom headgroup model [2].

4.2 *Molecular Orientation*

It is clear from Figure 4 the molecules are well aligned normal to the plane of the surface. At $A_m = 20.6$Å^2, the molecules are essentially upright, while at $A_m = 21.2$Å^2 they are tilted away from the surface normal. To quantify the ordering, we have calculated the distributions of three Euler angles which describe the orientation of a rigid molecule in the space-fixed frame.

The long-axis of the flexible amphiphile can be defined approximately in two

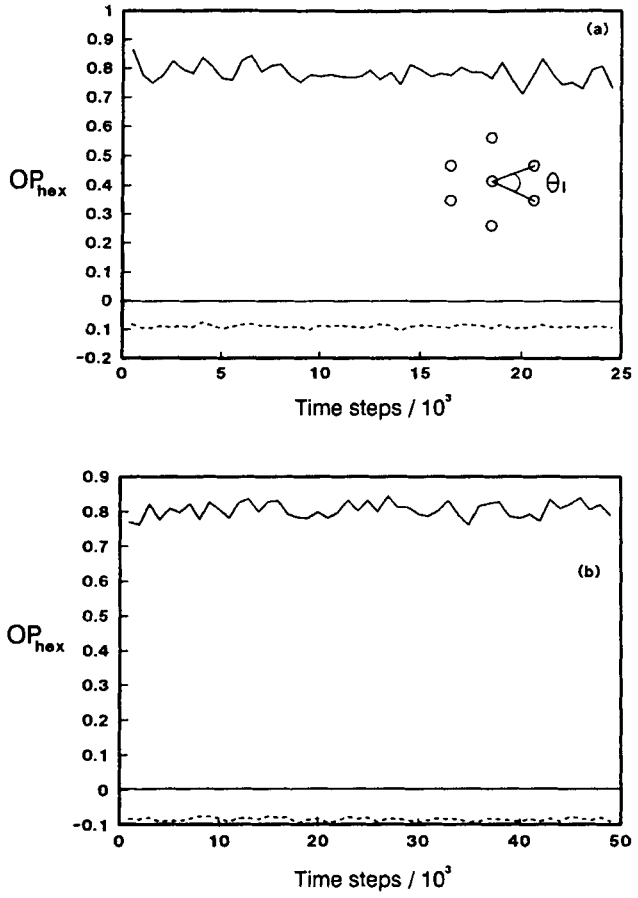

Figure 6 The hexagonal order parameter, OP_{hex}, as a function of time during the production phase of the simulations. The inset shows the definition of the angle θ_i used in equation (9). The real part of the order parameter is shown as a solid line and the imaginary part of the order parameter is shown a dashed line.

different ways. In the first method we use the vector between the carbon atom of the head-group and the carbon atom of the methyl group. In the second method the moment of inertia tensor of the amphiphile is diagonalised. This tensor is defined as

$$\mathbf{I} = \sum_{i=1}^{n} m_i(r_i^2\mathbf{1} - \mathbf{r}_i\mathbf{r}_i) \tag{10}$$

where $\mathbf{r}_i$ is the position of atom i from the molecular centre of mass and the sum is over all atoms in the molecule. The eigenvector corresponding to the smallest eigenvalue is the longest principal axis of the inertia tensor. The tilt angle, θ, of a molecule is defined as the angle between the long axis of the molecule and the surface normal.

The in-plane orientation of the layer is measured in terms of the azimuthal angle, ϕ, which is the angle between the projection of the long-axis onto the surface and the space-fixed x-axis defining one edge of the simulation box.

The twist angle, ψ, of the molecule is the angle between local x-axes and vector **R** defined by

$$\mathbf{R} = (-1)^n(\mathbf{r}_n - \tfrac{1}{2}(\mathbf{r}_{n-1} + \mathbf{r}_{n+1}))$$

which is the vector connecting the carbon atom C_n to the bisector of the vector joining the carbon atoms C_{n-1} and C_{n+1}. This is the rotation of the molecule about its own long axes. This simple definition of the twist angle of the molecule is only meaningful for molecules in which the hydrocarbon chain is in the all-trans conformation and we have only calculated this twist angle for these molecules.

Figure 7 shows the distribution, $n(\cos\theta)$ as a function of $\cos\theta$. The most probable tilt angle is at the maximum in $n(\cos\theta)$. The most probable molecular tilts are 2.4° and 18.8° for $A_m = 20.6\text{Å}^2$ and 21.2Å^2 respectively. The average tilt angle for the layer at $A_m = 21.2\text{Å}^2$ in the case of the single-atom head-group model is approximately 10° smaller than for the all-atom head-group at the same head-group area [2]. The slightly smaller effective head-group area of the single-atom head-group model would suggest that the model should exhibit a larger tilt than the all-atom head-group model. The most likely explanation is that the dipole image-dipole interaction increases the molecular tilt of the layer at low density. The image interaction produces a surface dipole which is anti-parallel to the real dipole and which has 60% of its magnitude. This is the dominant electrostatic interaction which minimised with a tilt around 20°.

The average azimuthal angle, ϕ, is shown as function of time in Figure 8(a) for the monolayer at $A_m = 21.2\text{Å}^2$. In contrast to the simulations with the single-atom head-group model the azimuthal angle remains essentially constant with time. The system does not attempt to explore the six degenerate ground states in which the molecule points towards the next-nearest neighbour molecules in the triangular lattice. The more realistic head-group head-group interactions of the all-atom head-group model lock the molecules into one azimuthal direction on the timescale of the simulation. The larger tilt angles found in the simulation of the all-atom head-group model also inhibit azimuthal rotation.

The distribution of azimuthal angles, calculated from both definitions of the long-axis, is shown in Figure 8(b) which shows that the average azimuthal angle is 91 ± 5°. Simulations with all-atom head-group model and the single-atom head-group model [2] both predict the next-nearest-neighbour orientation. Interestingly simulations with the united atom methylene groups [6, 7] predict a nearest neighbour tilt. Other simulations with the explicit hydrogen model [10] show that the tilting changes from nearest-neighbour to next-nearest-neighbour as a function of temperature. Diffraction studies of carboxylic acids on water exhibit phases with both orientations over a small temperature range [23]. The energy minimisation calculations of the all-atom head-group model also predict a next-nearest-neighbour orientation.

Figure 9 shows the distribution of molecular twist angles for the layer with $A_m = 21.2\text{Å}^2$. The layer has a lattice structure with two molecules per unit cell. These molecules are anti-parallel. This result contrasts with the one molecule per unit cell found for the single-atom head-group model.

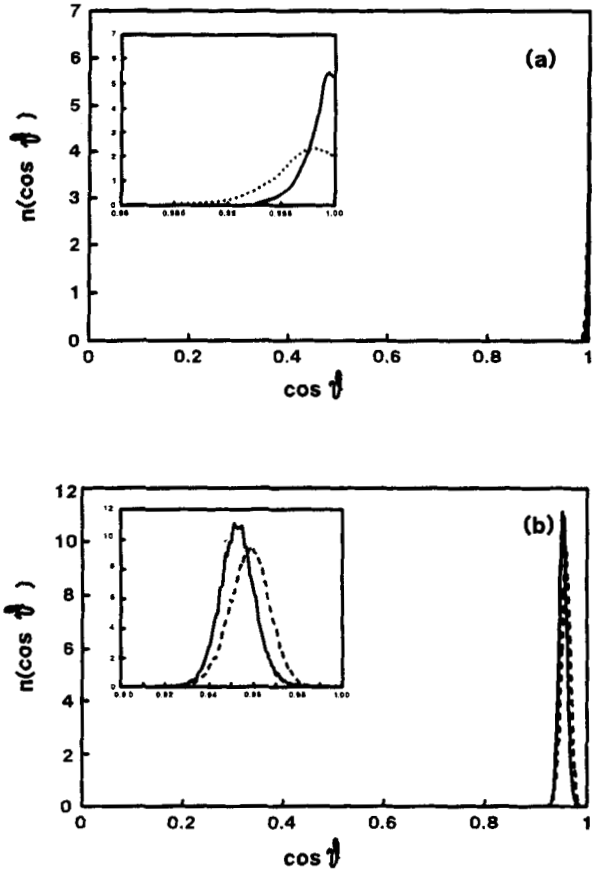

Figure 7 The distribution n(cosθ), which describes the average tilt of the molecules: (a) A_m = 20.6 Å^2; (b) A_m = 21.2 Å^2. End-to-end vector (dashed line), moment of inertia tensor (solid line).

4.3 *A calculation of the X-ray scattering pattern*

The structure factor for a set of N molecules containing m scattering centres is

$$S(\mathbf{k}) = \frac{1}{N}\langle \rho_k \rho_{-k} \rangle \tag{12}$$

where ρ_k is a Fourier component of the electron density; and $b_\alpha(k)$ is the X-ray scattering length of the atom which depends on $|\mathbf{k}|$. Within the

$$\rho_k = \sum_{i=1}^{N} \sum_{\alpha=1}^{m} b_\alpha(k) e^{-ik \cdot r_{i\alpha}} \tag{13}$$

periodic boundary conditions of the simulation k_x and k_y can only take restricted values, namely $k_x = 2\pi n/L_x$ and $k_y = 2\pi m/L_y$ where L_x and L_y are the box lengths

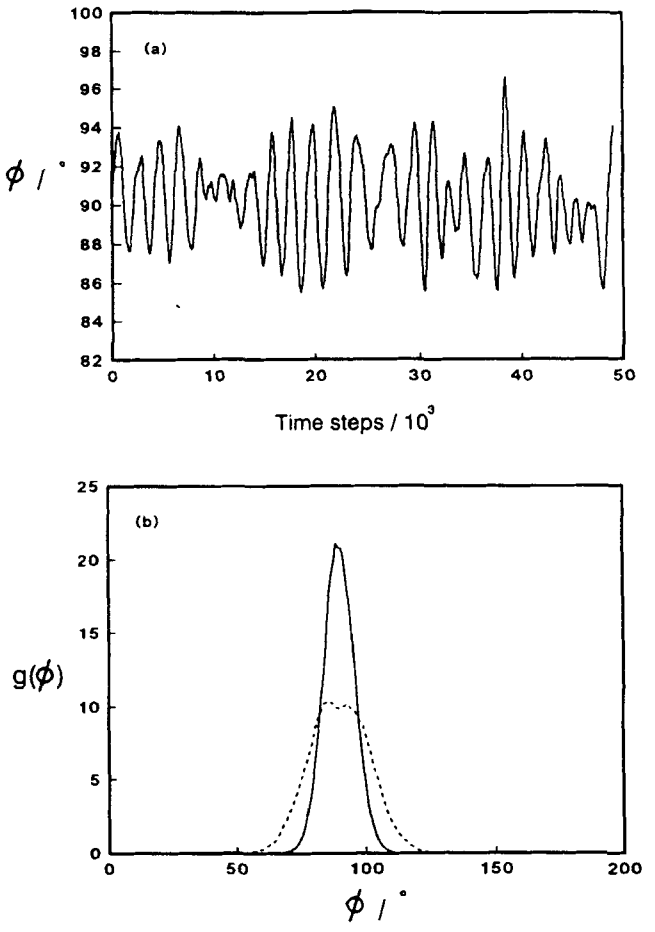

Figure 8 (a) The average azimuthal angle, ϕ, is shown as function of time for the monolayer at $A_m = 21.2$ Å^2. Figure 8(b) The distribution of azimuthal angles, calculated from both definitions of the long-axis. End-to-end vector (dashed line), moment of inertia tensor (solid line).

in the plane of the surface and n and m are integers. Figure 10 shows the structure factors for monolayers with $A_m = 20.6$Å^2 $A_m = 21.2$Å^2. The six sharp peaks closest to the origin are characteristic of the triangular structure of the adsorbate. At $A_m = 20.6$Å^2 there are two strong peaks and four weak peaks, whereas at $A_m = 21.2$Å^2 there are four strong and two weak peaks. To understand these modulations in intensity we have generated a number of idealized monolayer structures with different azimuthal and tilt angles. In these monolayers all molecules are in the all-trans configuration, the head-groups are at the same height and they form a perfect triangular lattice. The results of these calculations are summarised in table 7. The idealised monolayer in which the molecules tilt towards next nearest neighbour with $\theta = 20°$ (case (e)) show the four strong and two weak peaks characteristic of the molecular dynamics simulation at $A_m = 21.2$Å^2. The idealised

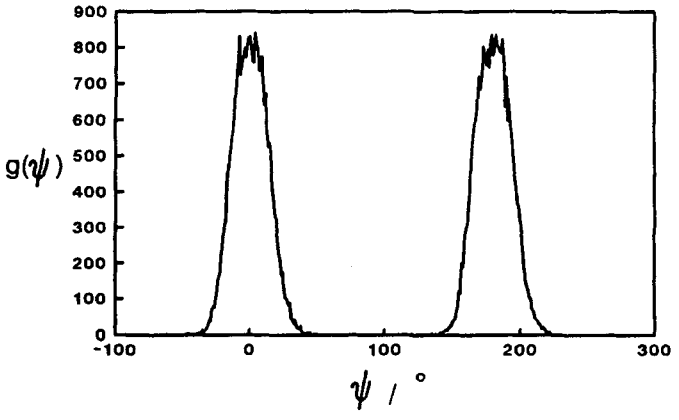

Figure 9 The distribution of molecular twist angles ψ for the monolayer with $A_m = 21.2$ Å^2.

Table 7 The structure factors for idealize monolayer structures. Two values of ψ indicate a two sublattice structure. s: strong; w: weak; vw: very weak.

Case	ϕ/°	θ/°	ψ/°	*S(k)*
(a)	0.0	0.0	0.0	2s, 4w
(b)	0.0	0.0	0.0/90.0	6s
(c)	0.0	20.0	0.0	2s, 4vw
(d)	0.0	20.0	0.0/90.0	2s, 4vw
(e)	90.0	20.0	0.0	4s, 2w
(f)	90.0	20.0	0.0/90.0	4s, 2w
(g)	90.0	20.0	0.0/90.0	4s, 2w

monolayer without tilt (case (a)) shows a structure factor with two strong and four weak peaks characteristic of the higher density simulation. The structure factors from previous united-atom simulations of arachidic acid [6, 7] which show a larger nearest-neighbour tilt ($\theta \approx 30°$), exhibit two strong and four weak peaks (case(c)). At present experiment does not help to resolve this difficulty. Measurements of the electron diffraction pattern of a stearic acid monolayer on an aluminium surface by Garoff *et al.* [24] show six sharp peaks with approximately equally intensity. This pattern would result if there was a uniform distribution of the short-axis of the amphiphile in the plane of the surface; figure (9) indicates that this is not the case. Equally if the molecules are upright in a two-sublattice herringbone structure (case (b)), the peaks are of approximately equal intensity. In our structures the twist angle distribution have maxima at $\psi = 0°$ and $\psi = 180°$ and there is no hint of a herringbone structure. Madden (*private communication*) has suggested that such an experimental pattern could be obtained from a one-sublattice tilted structure in which there are six equivalent domains (i.e. the nearest neighbour tilt directions are separated by sixty degrees). In this structure, long-range translational ordering would need to be preserved across the orientational grain boundaries. This appears to be the most likely explanation of the experimental diffraction pattern.

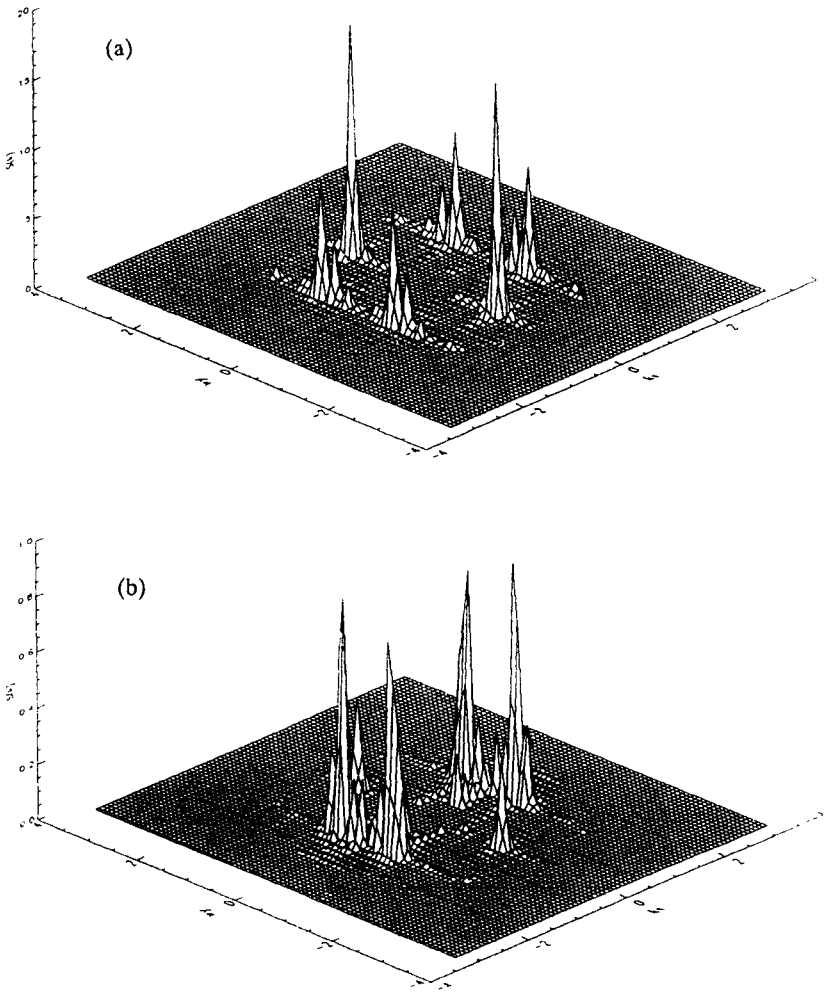

Figure 10 The X-Ray scattering patterns for the monolayer: (a) A_m = 20.6 Å^2; (b) A_m = 21.2 Å^2.

4.4 *The Distribution of Conformational Defects*

In considering the hydrocarbon chain, we define a gauche plus and gauche minus defect for dihedral angle between 60° and 180° and between −60° and −180° respectively. A C−C−C−C torsional angle of between −60° and +60° defines the trans state. The average number of molecules in the all-trans state was 97.7% at A_m = 20.6 Å^2, and 66.9% at 21.2 Å^2. Figure 11 shows the average distribution of gauche defect and carbon atoms, $\rho(z)$, along a direction normal to the surface. The first two sharp peaks in $\rho(z)$ correspond to the O1 and C1 atoms of Figure 1. The HD atom is shoulder on the low z side of the O1 peak. The O2 peak cannot be resolved. The sixteen methylene and one methyl group peak are clearly resolved

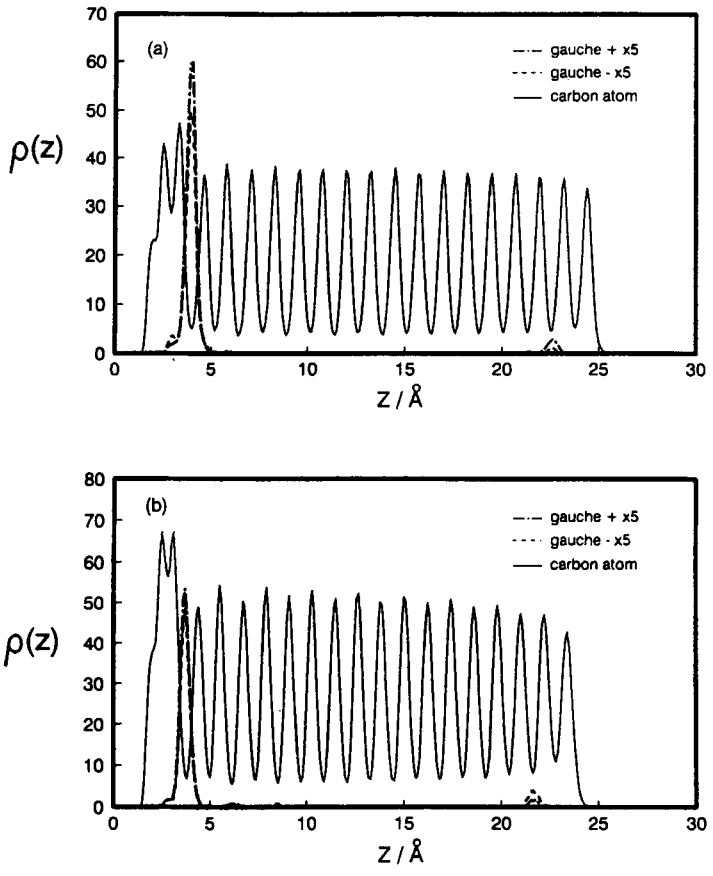

Figure 11 The average distribution of gauche defect (dashed line g^+, dotted line g^-) and carbon atoms, $\rho(z)$, (solid line) along a direction nominal to the surface: (a) $A_m = 20.6$ Å^2; (b) $A_m = 21.2$ Å^2. The distribution of gauche defects has been magnified by a factor of five for clarity.

and indicate that the molecules are well-ordered in the direction normal to the surface. The gauche defects at both densities are located at the ends of the chain near the head-group and the methyl tail. The large peak in these distributions at low-z results from the conformational freedom around the dihedral angle ϕ_{I+II} shown in Figure 1, where the notion of a gauche defect is not as meaningful as for the back-bone torsions. To explore this point more thoroughly, we have plotted the normalised distribution of torsional angles, $n(\phi)$, for the first four torsional angles moving away from the surface. This calculation is performed for the monolayer at $A_m = 20.6$ Å^2 and the results are shown in Figure 12. The change from a predominance of gauche-like states to trans states in moving up the chain is clear. Interestingly there is a similar gauche-like defect at same position in a stearic acid molecule in the B-form of the crystal which has a head-group area of 20.7 Å^2 [25].

One result of the preponderance of conformational disorder at the end of the chain is that the radial distribution functions and hexagonal order parameters of

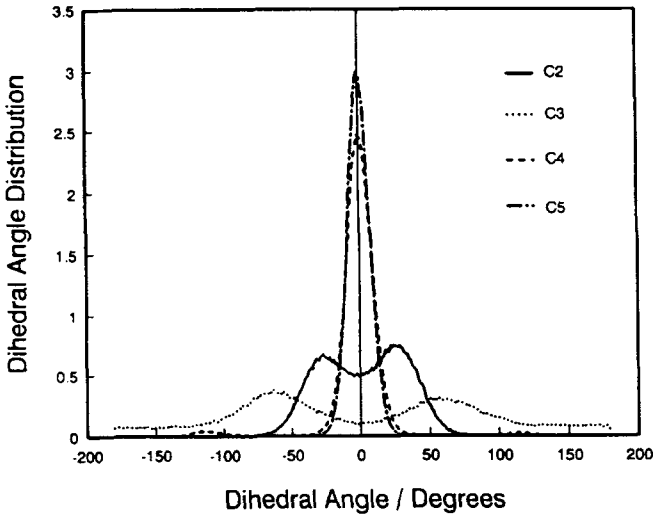

Figure 12 (a) The normalised distribution of torsional angles for the first four torsions in the chain for the monolayer at $A_m = 20.6$ Å^2: $\phi_{O1C1C2C3}$ ----; $\phi_{C1C2C3C4}$ ……; $\phi_{C2C3C4C5}$ ----; $\phi_{C3C4C5C6}$ —·—·

the head-groups and tails of the amphiphiles are quite liquid-like in comparison with the solid-like structure and order parameter obtained for the centre-of-mass of the chains. For instance, the OP_{hex} the head and tail groups are 0.51 ± 0.05 and 0.43 ± 0.06 for the layer at $A_m = 20.6$ Å^2 and 0.48 ± 0.1 and 0.22 ± 0.1 respectively for the layer at $A_m = 21.2$ Å^2. While the tail group in the layer of $A_m = 21.2$ Å^2 is hexagonally more disordered than the head group.

4.5 *Dipolar Orientation*

The important new feature of the all-atom head-group model is the dipole in the head-group, which controls the in-plane orientational ordering. The orientational distribution of dipole parallel and perpendicular to the surface plane have been calculated. The dipole vector is calculated from the partial charges.

$$\boldsymbol{\mu} = \sum_{i=1}^{n_c} q_i \mathbf{r}_i \tag{12}$$

where $\mathbf{r}_i$ is vector from the carbon atom of the head-group to one of the n_c charges in the molecule. The origin for the dipole in a neutral molecule is arbitrary. The direction of the vector is approximately parallel to the C=O bond and pointing from oxygen to carbon. Figure 13 and Figure 14 show the distribution of dipolar tilt angles and the distribution of dipolar azimuthal angle at both densities. Figure 12 shows that the dipoles in the layer are almost parallel to the surface. This maximises the attractive interaction with the image charges in the surface.

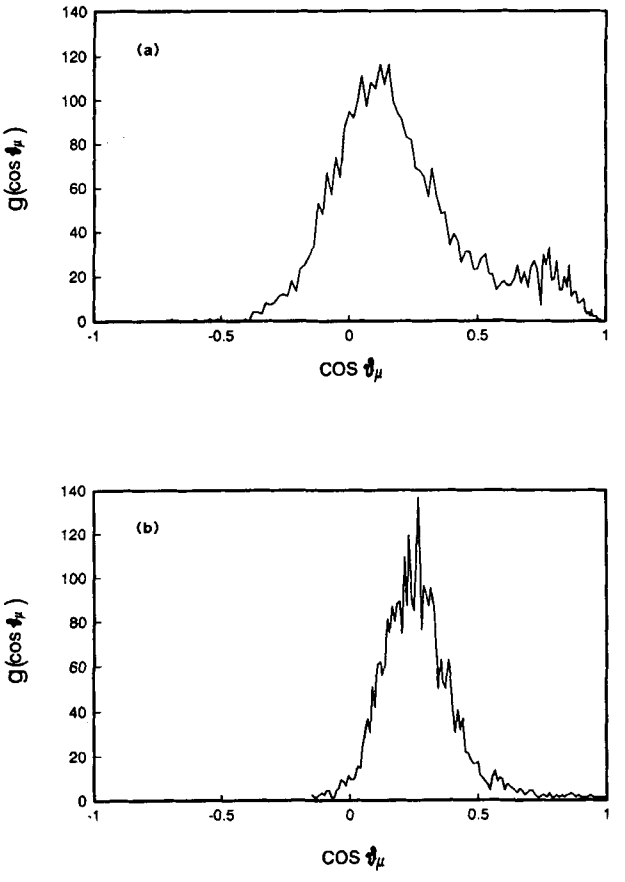

Figure 13 The out-of-plane tilt distribution of the dipoles: (a) A_m = 20.6 Å^2; (b) A_m = 21.2 Å^2.

The distributions of dipolar azimuthal angles is shown in Figure 14. At high density the molecules are aligned in a one sub-lattice structure with a relatively broad distribution. At the lower density, A_m = 21.2 Å^2, the dipoles form a two sub-lattice structure with the dipoles oriented parallel to the surface. Dipoles in alternate rows are anti-parallel.

6 CONCLUSIONS

Energy minimisation calculations and molecular dynamics simulation using the all-atom model have been carried out to predict the detailed structure and dynamics of a model Langmuir-Blodgett monolayer on a hydrophilic surface. The all-atom model contains a more realistic model of the head-group/head-group and the head-group/surface potential. The addition of a realistic electrostatic interaction has little effect on the minimum energy structure. The tilting transition is shifted to slightly

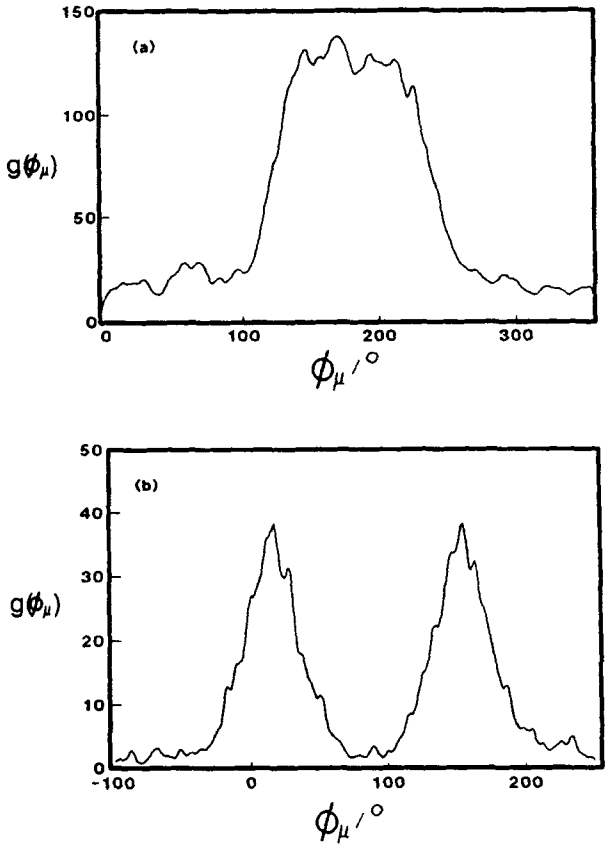

Figure 14 The in-plane azimuthal distribution of dipoles: (a) $A_m = 20.6$ Å^2; (b) $A_m = 21.2$ Å^2.

lower head-group areas per molecule due to the larger effective cross section of the all-atom head-group. The detailed structure of the monolayers at 300 K is significantly different from that predicted by the simpler single-atom head-group model [2]. The all-atom model predicts significant conformational disorder at the torsion connecting the carboxylic acid head-group and alkyl chain of the molecule. This defect is also observed in the B-form of the stearic acid crystal. The distribution of the molecular centres of mass is solid-like, while the distribution of the gauche defects is liquid-like. The molecular tilt of the layer of $A_m = 21.2$ Å^2 is 18.8°, which is double the value of 9° for the single-atom head-group monolayer and much closer to the tilt angle obtained from the energy minimisation calculation and to the value obtained from X-ray scattering on Langmuir films [26]. The dipoles of the head-group are aligned parallel to the surface and in the tilted phase the dipoles form a two sub-lattice structure in the plane of the surface.

Acknowledgements

K.S.K. would like to thank BP plc for a studentship. The computational work described in this paper was carried out under grant GR/F/51867 from the Computational Science Initiative of the SERC.

References

[1] G.G. Roberts, Langmuir Blodgett films. Plenum Press, (1990).
[2] M.A. Moller, D.J. Tildesley, K.S. Kim and N. Quirke, "Molecular dynamics simulation of a Langmuir Blodgett film", *J. Chem. Phys.*, **94**, 8390 (1991).
[3] A.J. Kox, J.P.J. Michels and F.W. Wiegel, "Simulation of lipid monolayer using molecular dynamics", *Nature*, **287**, 317 (1980).
[4] P. van der Ploeg and H.J.C. Berendsen, "Molecular dynamics simulation of a lipid bilayer", *J. Chem. Phys.*, **76**, 3271 (1982).
[5] J.P. Ryckaert and A. Bellemans, "Molecular dynamics of liquid alkanes", *Faraday Discussions of the Chem. Soc.* **66**, 95 (1978).
[6] J.P. Bareman, G. Cardini and M.L. Klein, "Characterization of structural and dynamical behaviour in monolayers of long chain molecules using molecular dynamics calculations", *Phys. Rev. Letts*, **60**, 2152 (1988).
[7] G. Cardini, J.P. Bareman and M.L. Klein, "Characterization of Langmuir-Blodgett monolayers using molecular dynamics calculations", *Chem. Phys. Letts*, **145**, 493 (1988).
[8] J.G. Harris and S.A. Rice, "A molecular dynamics study of the structure of a model lipid monolayer of amphiphilic molecules", *J. Chem. Phys.*, **89**, 5898 (1988).
[9] A. Ulman, J.E. Eilers and N. Tilman, "Packing and molecular orientation of alkanethiol on gold surfaces", *Langmuir*, **5**, 1147 (1989).
[10] J.P. Bareman, M.L. Klein, "Collective tilt behaviour in dense substrate-supported monolayers of long chain molecules: a molecular dynamics study", *J. Phys. Chem.*, **94**, 5202 (1990).
[11] J. Hautman and M.L. Klein, "Simulation of monolayers of alkanethiol chains", *J. Chem. Phys.*, **91**, 4994 (1989).
[12] Fois, E., and Madden, P.A., 1991, *private communication*.
[13] J. Hautman, J.P. Bareman, W. Mar and M.L. Klein, "Molecular dynamics simulation of self-assembled monolayers, *J. Chem. Soc. Faraday Trans.*, **87**, 2031 (1991).
[14] J.P. Ryckaert, "Special geometrical constraints in the molecular dynamics of chain molecules", *Mol. Phys.*, **55**, 549 (1985).
[15] N.L. Allinger, "Conformational analysis. 130. MM2. A hydrocarbon force field utilizing V_1 and V_2 torsional terms" *J. Amer. Chem. Soc.*, **99**, 8127 (1977).
[16] S.J. Weiner, P.A. Kollman, D.A. Case, U.C. Singh, C. Ghio, G. Alagona, S. Profeta Jr. and P.K. Weiner, "A new force field for simulations of proteins and nucleic acids", *J. Amer. Chem. Soc.*, **106**, 765 (1984).
[17] S.J. Weiner, P.A. Kollman, D.T. Nguyen and D.A. Case, "An all atom force field for simulations of proteins and nucleic acids", *J. Comp. Chem.*, **7**, 230 (1986).
[18] J. Hautman and M.L. Klein, "An Ewald summation method for planar surfaces and interfaces", *Mol Phys.*, **75**, 379 (1992).
[19] G.M. Torrie, J.P. Valleau and G.N. Patey, "Electrical double layers II. Monte Carlo and HNC studies of image effects", *J. Chem. Phys.*, **76**, 4615 (1982).
[20] R.C. Weast and M.J. Astle, CRC Handbook of Chemistry and Physics, 63rd edition, E-56 (1983).
[21] M. Bishop and J.H.R. Clarke, "System size dependence and time convergence in molecular dynamics simulation of monolayer films", *J. Chem. Phys.*, **95**, 540 (1991).
[22] M.P. Allen and D.J. Tildesley, Computer Simulation of Liquids, Clarendon Press, Oxford (1987).
[23] A.M. Bibo and I.R. Peterson, "Disclination recombination kinetics in water surface monolayers of 22-tricosenoic acid", *Thin Solid Films*, **178**, 293 (1989).
[24] S. Garoff, H.W. Deckman, M.S. Dunsmuir, M.S. Alvarez and J.M. Bloch, "Bond orientational order in Langmuir-Blodgett surfactant monolayer", *J. Phys. (Paris)*, **47**, 701 (1986).
[25] M. Goto and E. Asada, "The crystal structure of the B-form of stearic acid", *Bull. Chem. Soc. Jpn.*, **51**, 2456 (1978).
[26] K. Kjaer, J. Als-Neilsen, C.A. Helm, P. Tippman-Krayer and H. Möhwald, "Synchrotron X-ray diffraction and reflection studies of arachidic acid monolayers at the air water interface", *J. Phys. Chem.*, **93**, 3200 (1989).